

Multiscale Skeletonization: An Electrostatic Field-Based Approach ¹

Gamal Abdel-Hamid² and Yee-Hong Yang³
Computer Vision Laboratory, Department of Computational Science
University of Saskatchewan, Saskatoon, Saskatchewan, Canada S7N 0W0
Email Address for Y.H. Yang: yang@cs.usask.ca
Phone Number for Y.H. Yang: (306) 966-4891
Fax Number for Y.H. Yang: (306) 966-4884

December 14, 1994

Abstract

Skeleton representation of an object is believed to be a powerful representation that captures both boundary and region information of the object. The skeleton of a shape is a representation composed of idealized thin lines that preserve the connectivity or topology of the original shape. Although the literature contains a large number of skeletonization algorithms, many open problems remain. In this paper, a new skeletonization approach that relies on the Electrostatic Field Theory (EFT) is proposed. Many problems associated with existing skeletonization algorithms are solved using the proposed approach. In particular, connectivity, thinness, and other desirable features of a skeleton are guaranteed. Furthermore, the electrostatic field-based approach captures notions of corner detection, multiple scale, thinning, and skeletonization all within one unified framework. Experimental results are very encouraging and are used to illustrate the potential of the proposed approach.

¹The authors would like to acknowledge financial support provided by NSERC through grant number OGP0000370.

²Gamal Abdel-Hamid passed away on Dec. 4, 1994

³To whom correspondence should be addressed.

I. Introduction

Shape representation and description plays an important role in most computer vision systems. A useful and reliable shape representation must meet a number of requirements, which include *invariance*, *uniqueness*, and *stability* [21, 22]. If two objects have the same shape, then their representations should be the same and should be invariant with respect to translation, rotation and scaling. Uniqueness means that if two objects have different shapes they should have different representations. Stability denotes the fact that if two objects have a small shape difference, then their representations should have a small difference. Conversely, if two representations have a small difference, then the objects they represent should also have a small shape difference. Therefore, a stable representation means a representation that is insensitive to noise. In short, the object shape and its representation should have a one-to-one correspondence property. Also, the representation should reflect the shape of the object at various levels of abstraction. The representation should also combine both boundary and region information of the object. Finally, the representation and the recognition of objects, which employ this representation should be computable efficiently. Other criteria for shape representation can be found in reference [22]. Skeleton representation as introduced by Blum [3] is a representation that meets most of the aforementioned requirements. The skeleton of a two-dimensional object is a transformation which maps the contour of the object into a one-dimensional line representation similar to that of a stick figure.

Since the introduction of the skeleton representation, many skeletonization algorithms have been reported in the literature [30]. Many problems, however, remain unsolved. For example, methods to quantitatively evaluating skeletons are still lacking. Recently, the work done by Suen and his colleagues in skeleton evaluation is an exception [13, 15, 26].

Another problem with most skeletonization algorithms is their sensitivity to noise. Although there are many skeletonization algorithms, little work has been directed towards studying the sensitivity of these algorithms to boundary noise. Also, some existing skeletonization approaches require many parameters to be supplied by the user [16].

In this paper, a new skeletonization approach, which is developed based on the Electrostatic Field Theory (EFT), is proposed. The motivation of this research work stems from the following reasons. First, the encouraging results of a recently developed corner detector based on the same underlying theory, the EFT [1], suggest the possibility of applying the EFT to determine skeletons. In reference [1], it was pointed out that electrostatic field lines represent lines of symmetry naturally. Secondly, EFT presents a natural solution for skeletonization which can overcome many of the difficulties, e.g., connectivity and noise sensitivity of existing approaches. Thirdly, EFT unifies notions of corner detection, thinning, skeletonization, and multiple scale, all within the same framework.

The paper is organized as follows. An overview of the related research is discussed in Section II. The relevant background on the EFT is reviewed in Section III. The proposed approach for skeletonization is presented in Section IV. In Section V, the experimental procedure that is used to evaluate skeletons is described. The experimental results conducted to demonstrate the potential of the EFT-based skeletonization algorithm are given in Section VI. Section VII draws a comparison between the proposed approach and a recently published approach and highlights some of the merits of the proposed approach. Finally, conclusions and future work are presented in Section VIII.

II. Related Work

This section gives to a brief review of skeletonization algorithms along with their main characteristics and drawbacks. For a more complete survey of skeletonization algorithms in general, the interested reader can consult reference [30].

Existing skeletonization approaches can be classified approximately into a small number of categories. The first category is based on *topological* or *direct thinning*. Thinning denotes the process of iteratively peeling away the object's contour pixels while preserving its topology [14]. Many thinning algorithms have been developed both as sequential [7] and parallel [10] algorithms. The drawbacks of thinning algorithms are noise sensitivity, loss of continuity, and distortion which usually leads to

counterintuitive results. Therefore, most thinning algorithms have been directed towards character recognition applications. The reader may refer to reference [14] for a comprehensive survey and bibliography of thinning algorithms.

The second category is to compute the symmetric axes using *direct*, or *analytical* methods by approximating the object's boundary by a polygon. For noisy or biological (as cells) objects, this approximation leads to unavoidable inaccuracy. Algorithms belonging to this category are based on either heuristic methods [2, 18, 28] or more rigorous methods such as Voronoi diagram [4, 24]. Although this category has many advantages over thinning algorithms (since they make measurements of Euclidean distance in the continuous domain rather than in the digital grid), the algorithms in this category are of little practical use mainly because of their computational complexity (for example, the Voronoi diagram).

The third category of skeletonization algorithms is the *ridge following* algorithms. A *Distance Transform* (DT) is applied to the object shape, from which ridges are found. The projection of these ridges constitute the skeletal branches of the object. Ridges can be traced by the active contour model [16] and by other methods [9]. Also different DT's have been used in the literature. (See [16] for a survey.) Algorithms in this category are relatively simple. In general, the skeletonization results of this category are more accurate and are smoother than those of the other two categories [16]. A major drawback of algorithms in this category is that the DT of an object is, in general, sensitive to noise. Equidistance contours are as noisy as the boundary. Representative examples of this category can be found in references [6, 12].

Although our proposed approach for skeletonization cannot fit rigidly into any of the aforementioned categories, it has some commonalities with algorithms in the ridge following category, where the DT is replaced by an *electrostatic potential surface transform* and the ridge following process by the tracing of field lines passing through significant convexities and concavities detected along some equipotential contour. The potential distribution of an object is obtained by solving the Poisson equation inside the object. The Poisson equation has been used before to model and solve computer vision problems such as the lightness problem, shape-from-shading, and the computation of optical flow [29]. The proposed potential surface approach can represent the object's shape at different levels of smoothing or scale and can capture important shape information such as curvature. Furthermore, equipotential contours are smoother than equidistance contours which are employed in the ridge following category. Advantages of the proposed skeletonization approach are discussed in Section VII.

III. Background on the Electrostatic Field Theory (EFT)

This section reviews the relevant concepts of the EFT.

General Properties of Electrostatics

The following are some of the properties of electrostatic potential and field:

1. The electrostatic potential, $v(x, y)$, at a point (x, y) in the 2-dimensional space R^2 is governed by the Poisson equation

$$\nabla^2 v = -\frac{\rho_{vf}}{\epsilon},$$

where ∇^2 is the *Laplacian* operator, ρ_{vf} is the free charge density at (x, y) , and ϵ is the permittivity of the medium.

2. The electrostatic field intensity vector $\vec{E}(x, y)$ at (x, y) can be computed from the potential $v(x, y)$ using the following expression:

$$\vec{E} = -\nabla v.$$

Two observations can be made. First, the field is in the direction of the steepest descent of the potential. Second, the field lines are perpendicular to the equipotential contours and are directed from the high to the low potential.

3. A pure conductor is an equipotential surface and the electrostatic field vector \vec{E} is zero everywhere inside the conductor. The electrostatic field on the conductor surface, however, may be nonzero and is given by

$$\vec{E}_s = \frac{\sigma_s}{\epsilon_0} \hat{n},$$

where σ_s is the surface charge density, ϵ_0 is the permittivity, and \hat{n} is an outward unit vector normal to the surface of the conductor.

4. The electrostatic field distribution on the conductor surface is proportional to the local curvature of the conductor surface, which has been verified both theoretically and experimentally [1],[20]. This means that the electrostatic field conveys the same information as the curvature of an object boundary. Electrostatic field extrema along an equipotential contour correspond to curvature extrema (significant convexities and concavities). This property is the main motivation behind using the EFT to extract the skeleton of an object and has been exploited in [1] to detect corners.
5. The field lines are normal to a conductor boundary. At a corner, the field lines are directed along the bisector of the angle of the corner. This property is very important and suggests that the electrostatic field lines can represent lines of symmetry and hence the skeleton.

IV. Electrostatic Field-Based Approach to Skeletonization

The input to the proposed skeletonization approach, which is similar to most skeletonization approaches, is the binary image of an object. In the proposed approach, a skeleton is defined as the electrostatic field lines passing through points of significant convexities and concavities. The following are the steps required to find the skeleton of a planar object:

1. Compute the potential distribution $v(x, y)$ inside the object,
2. Find the equipotential contour at a given potential v_{con} ,
3. Detect significant convexities and concavities along an equipotential contour, and
4. Trace skeletal points starting from points of significant convexities and concavities.

The following subsections give details of each of the above steps.

A. Solution of the Potential Distribution Inside the Object

To find the potential distribution inside the object is the most important step in the proposed skeletonization algorithm. It resembles, in some sense, the distance transform step in the ridge following approach [16]. Assume that the planar object has no holes. The space between the object and the image border (non-object area) is modeled as a conductor of electrostatic potential v_b and the interior region as a cavity in the conductor having a dielectric of permittivity ϵ (see Figure 1). If the cavity is free of charge, the electrostatic field will be zero everywhere inside the cavity and the potential inside the cavity will be v_b . In the proposed approach, the cavity is charged with a negative charge density ρ_{vf} so that the electrostatic field can exist inside the cavity. The problem of finding the potential distribution inside the cavity is a boundary value problem, commonly known as the *interior Dirichlet problem* for solving the Poisson equation [31]. (The exterior Dirichlet boundary value problem for the Laplace equation was employed in [1] for

the detection of corners.) It can be easily verified that the solution is unique. Many methods for the solution of the interior Dirichlet boundary value problem have been reported in the literature. Both iterative [11] and direct analytical [29] solutions have been used to solve vision problems such as the lightness problem, the shape-from-shading problem, and the computation of optical flow. In this paper, the Jacobi relaxation method [31] is adopted because of its simplicity.

In a digital grid, the Laplacian operator is approximated by the finite difference method as follows:

$$\nabla^2 v = \frac{\partial^2 v}{\partial x^2} + \frac{\partial^2 v}{\partial y^2} = \frac{1}{\Delta^2}(v_{i-1,j} + v_{i,j-1} + v_{i+1,j} + v_{i,j+1} - 4v_{i,j}),$$

where Δ is the spacing between picture cell centers. Let $\Delta = 1$ for convenience. The potential at point (i, j) at iteration k , $v_{i,j}^k$, is given by:

$$v_{i,j}^k = \frac{1}{4}(v_{i+1,j}^{k-1} + v_{i-1,j}^{k-1} + v_{i,j+1}^{k-1} + v_{i,j-1}^{k-1} + \frac{\rho_{vf}}{\epsilon}),$$

where all the values used in these calculations are floating point numbers. Notice that the potential for a point at the i th iteration is merely dependent on the potential of its vertical and horizontal neighbors at the $(i - 1)$ th iteration.

The iteration terminates when the potential distribution stops changing after N iterations, i.e., when the following condition is satisfied

$$\sum_{i,j} |v_{i,j}^N - v_{i,j}^{N-1}| = 0.$$

Recall that ρ_{vf} is constant everywhere inside the cavity (object region). It is noteworthy that the value of this constant ρ_{vf} does not affect the potential distribution generated except for a scale factor. This has been verified experimentally and can be easily seen because the Poisson equation is linear. Hence, after the final potential distribution is computed, the potential distribution is normalized as follows. The maximum potential v_b of the object boundary is set equal to 255 and the minimum potential is set equal to 0 and the potential values inside the object is computed using a simple linear transformation. The potential distribution of an object is a characteristic surface of the object and does not depend on any parameters.

The computed surface $S = v_{i,j}$ represents the potential surface of the object that will be utilized for the construction of the skeleton. Figure 2 demonstrates the potential surface generated for the image of a Maple leaf. The potential surface possesses a number of interesting and useful properties which are outlined in Section VII.A in comparison with the Euclidean distance transform.

B. Construction of an Equipotential Contour at a Given Potential

The equipotential contour is used to detect significant convexities and concavities along the contour from which skeletal branches are initiated. This step can be visualized as a potential surface $S = v(x, y)$ being cut by a constant potential plane (parallel to the x-y plane). The curve that results from the intersection of the potential surface and the cutting plane is a closed contour. In the implementation, it is expressed as a Freeman chain code. Since the spatial domain is a digital grid and the potential distribution takes on floating point values, the construction of a connected equipotential contour at a given potential, v_{con} within the range $0 - 255$, can be computed as follows.

First, all pixels having a potential less than or equal to v_{con} are marked. The marked region is guaranteed to be a single connected region. Second, the boundary of the marked region is traced in a clockwise direction and these boundary pixels are labeled in a Freeman chain code. As the boundary is traversed, the location, at subpixel resolution, of the point at which the potential is exactly equal to v_{con} is found by using the bilinear interpolation (see [5] for details). By connecting the locations (at subpixel resolution) having a potential exactly equal to v_{con} , the required equipotential contour is constructed. The corresponding field values at each of this chain of points are also computed

simultaneously for later processing. In this way, the one-dimensional relation between the field E along the contour and the corresponding arc length s , measured with reference to some arbitrary fixed point on the contour, is found. The arc length is normalized with respect to the total contour length such that s takes on values in the range $[0 - 1]$. Thus the result of this step is a one-dimensional curve $E(s)$ at the given potential v_{con} . It is worth noting that the lower is the value of contour potential v_{con} , the smoother the contour, the smoother the curve $E(s)$, the less the number of extrema of the field, and the less the number of significant convexities and concavities as expected due to the smoothing effect of the solution of the potential distribution inside the object. Figure 3 illustrates this effect by depicting the field distribution along different equipotential contours for the image of a Maple leaf with the boundary corrupted with Gaussian noise of $\sigma = 3$.

From the above discussion, it is evident that the proposed skeletonization approach has the advantage of a multiscale approach. By appropriately choosing the equipotential contour at potential v_{con} , the desired level of details (or scale) of the skeleton can be selected. In particular, choosing an equipotential with a low value of v_{con} , a coarse skeleton is generated, whereas choosing an equipotential with a high value of v_{con} , a fine skeleton is generated. This multiscale feature of the proposed approach is attributed to the natural smoothing characteristic of the Poisson equation. Such a smoothing effect has been used previously in reconstructing the three-dimensional default shape of an object from its occluding contour [33]. Figure 4 shows this interesting property of the potential distribution by depicting some equipotential contours of the Maple leaf at various potentials.

C. Detecting Corners along the Equipotential Contour

Starting from the field distribution $E(s)$ along the contour s , convex (concave) corners are allocated by identifying points having local minima (maxima) of the field $E(s)$. Locations of minima (maxima) of the field are identified as convex (concave) corners [1]. As mentioned in the previous step, the choice of the contour potential v_{con} directly determines the degree of detail of the skeleton. Figure 5 demonstrates this fact by depicting different equipotential contours and their associated detected corners. The lower is the potential, the lower the number of corners detected. It should be noted that the interaction corner models discussed in reference [27], namely, the Γ , the *End*, and the *Stair* models, are also apparent in the EFT-based approach [1] and can be observed in Figure 5. For example, corners merging, disappearing, attracting, and repelling can be seen in the figure.

In this paper, both convex and concave corners are employed in generating skeleton branches. Many skeletonization algorithms consider only convex corners (e.g. [7]). Considering only convexities may be justified in certain applications as in the identification of pseudopods [7], but, both convexities and concavities must be considered because both contribute equally to the shape of an object. For a unique skeleton representation (see Section II), both convexities and concavities must be considered (see Figure 6).

D. Skeleton Tracing

Having identified points of significant convexities and concavities along an equipotential contour at a potential v_{con} , these points are used to initiate the skeleton tracing procedure. The skeleton branches correspond to field lines passing through significant corners identified in the previous step. So the skeleton generation procedure is reduced to the problem of tracing the field lines. Starting from the points having significant convexities and concavities along an equipotential contour of potential v_{con} , the field lines are traced in two directions; 1) in the inward direction towards the object's central region or pixel, in the potential range $v_{con} - 0$, and 2) in the outward direction towards the object's boundary, in the potential range $v_{con} - v_b$. When tracing inward, the process is simulated by initially putting a positive charge in the identified location of the convexity (or concavity) pixel. The positive charge, under the influence of the electrostatic field, favors to move in the direction that minimizes its energy. Such a direction is also the direction of the electrostatic field. In the implementation, the charge is allowed to move in an $n \times n$ neighborhood in each iteration, where n is an odd integer and it determines the angular resolution of the field lines.

The larger is n , the finer the angular resolution. Using too small a window (e.g. 3×3), leads to jaggy skeletal branches due to inaccurate tracing of field lines in the digital grid. On the other hand, using too large a window (e.g. 11×11) also results in poor tracing of the field lines since a skeletal branch will be broken into line segments of length $\lfloor \frac{n}{2} \rfloor$. A 7×7 window seems to be a good choice (see Figure 7). In each iteration, $\lfloor \frac{n}{2} \rfloor$ pixels in the $n \times n$ window are marked. Pixels that are traced by the charge while it is moving are marked as skeletal pixels. This tracing process terminates when the charge hits the object's central pixel or region at zero potential, thus reaching its global minimum energy. It is noteworthy that the skeletal branches generated by this procedure is guaranteed to meet at the center or at the minimum potential region since the potential distribution decreases monotonically in the inward direction up to the central point of zero potential. Also the connectivity requirement of the skeleton is guaranteed using this approach because field lines must be continuous.

In principle, the same process could be used in the outward direction towards the object's boundary by replacing the positive charge with a negative charge. Also pixels traced by the charge movements could be marked as skeletal pixels. The process could then terminate when the charge hits the object's boundary at a potential v_b (or 255), thus reaching its global minimum energy. Looking at Figure 7, however, it can be observed that the outward tracing part of the field lines is not accurate enough to make the charge hit the corner at the desired boundary location. This deviation of field lines occurs only for sharp convex corners since the region of support for estimating the field direction (the gradient direction) is not large enough to compute the field direction correctly as the charge approaches the boundary and hence, the charge tends to deviate and take the shortest path to the boundary. The problem is not inherent in the EFT but is a result of quantization. In the implementation, the following mechanism is employed to alleviate this problem. Instead of tracing the field lines in the outward direction by the moving charge, the field extrema of adjacent contours are matched. This leads to more accurate tracing of the field lines in the outward direction as can be seen by comparing Figure 7(c) and (d).

V. Experimental Procedure for Evaluating Skeletons

Despite the large number of skeletonization algorithms developed so far, the literature lacks algorithms for evaluating skeletons quantitatively. Suen and his colleagues, however, made some effort in this direction [13, 15, 26]. In reference [13], Lam and Suen use three different but somehow correlated measures of distance between the constructed skeleton and a reference (ideal) skeleton that has been prepared manually. In this paper, a similar distance measure is adopted. For each skeletal pixel, the distance between the skeletal pixel and its ideal position given by the ideal skeleton is computed. Because the goal of the evaluation procedure is to study the behavior of the proposed skeletonization approach in the presence of noise, shapes with known ideal skeletons are used, e.g. a square. The distance value takes on either positive or negative value depending on which side the skeleton point lies with respect to the ideal skeleton's branch. This distance measure is similar to the projection distance employed in [13]. The variance of the distance array $x_i, 1 \leq i \leq N$, is computed as follows:

$$V(X) = E(X^2) - E^2(X),$$

where

$$E(X) = \frac{1}{N} \sum_{i=1}^N x_i,$$

and

$$E(X^2) = \frac{1}{N} \sum_{i=1}^N x_i^2.$$

$E(X)$ denotes the expected or the average projection distance, $E(X^2)$ denotes the mean squared projection distance, and N is the number of skeletal pixels. The standard deviation, SD, is then

calculated from the variance

$$SD(X) = \sqrt{V(X)}.$$

The standard deviation is thus used as the figure-of-merit of the skeleton evaluated. The smaller is the value of the SD, the closer the skeleton to the reference skeleton.

VI. Experimental Results

Both synthesized and real objects were used in the experiments. For the synthesized objects, an image of a 63×63 pixels square centered on a 128×128 image is used. The ideal skeleton of this square is the two intersecting diagonal lines. To test the sensitivity of the proposed EFT-based skeletonization approach with respect to boundary noise, the boundary of the square is perturbed by varying degrees of zero-mean Gaussian noise. The standard deviation σ of the noise is varied in the range from 0 to 4 in steps of 0.2 units. The square’s boundary is kept at a potential of $v_b = 255$. The skeletons are generated starting at equipotentials in the range 140 – 200 in steps of 5. Figure 8 depicts a three-dimensional graph showing the variation of the SD at varying levels of boundary noise and starting potentials.

Some observations and remarks can be drawn from the figure. First, it can be noticed that the SD increases with the boundary noise, a finding which agrees with one’s intuition. Secondly, except for a few erratic spikes in the figure, the SD is kept at a reasonably low level even at a noise level of 4. This result is quite encouraging since it illustrates the insensitivity of the proposed skeletonization algorithm to boundary noise. The erratic spikes appearing in the figure are attributed to the false corners detected due to the severe boundary noise. These false corners generate extra branches that contribute significantly to increasing the value of the SD. This problem is under investigation by the authors and is beyond the scope of this paper.

The skeletons generated starting at a potential of 170 at different noise levels are depicted in Figure 9. Despite the severe boundary noise, the skeletons generated at noise levels 2 and 4 are very close from the ideal one.

To see the performance of the proposed skeletonization algorithm when applied to real images, the algorithm is experimented with an image of a Maple leaf. Figures 10(a) and (b) illustrate the skeletons generated for the Maple leaf starting at potentials of 190 and 150, respectively. The comparison of the skeletons generated at different starting potentials demonstrates clearly the multiscale capability of the proposed skeletonization algorithm. The skeleton generated at a potential of 150 (Figure 10 (b)) is coarser in scale and hence, has a smaller number of branches when compared to that generated at a potential of 190 (Figure 10 (a)).

VII. Discussion

In this section, a comparison between the potential surface and the Euclidean distance transform is presented. Potential Distribution versus Distance Transform

The following lists some of the similarities of the potential surface generated by the EFT and the Euclidean distance transform:

- Both transforms are based on the solution of a partial differential equation. The Euclidean distance transform is generated based on solving the *Eikonal equation* $(\nabla D)^2 = (\frac{\partial D}{\partial x})^2 + (\frac{\partial D}{\partial y})^2 = 1$ inside the planar object, where $D(x, y)$ is the distance from a point inside the object, (x, y) , to the boundary, while the potential surface is generated based on the solution of the Poisson equation inside the object.
- Both surfaces are monotonically decreasing with respect to the center of the object, and hence, there is only one equipotential contour for a given potential and one equidistance contour for a given distance. (Note that this is true only for objects containing no holes).

- Both transforms capture the geometric symmetries of planar objects and this is the reason behind their usage in extracting skeletons.
- Both transforms are fundamental to their corresponding skeletonization approaches.

However, the two transforms can be contrasted in the following points:

- Each transform is based on a different equation as mentioned before. The Eikonal equation attempts to find a distance distribution, $D(x, y)$, such that the magnitude of the gradient is uniform everywhere inside the object while the Poisson equation (with uniform ρ) tries to find a potential distribution such that the Laplacian of the potential is uniform.
- The solution of the Poisson equation under the given boundary conditions (the interior Dirichlet boundary problem) is unique [31]. In the case of the Eikonal equation, however, both $D(x, y)$ and $-D(x, y)$ are possible solutions.
- The proposed potential surface reflects the shape of the object more naturally than the Euclidean distance transform. The potential surface represents what might be called “the evolution” or “the history” of the object. The center of the object (pixel or contour of zero potential) represents the starting phase of the object as a nucleus and the equipotential contours of increasing potential represents the evolution history of the object until all the details develop in the final phase of the object (see Figure 4).
- The Poisson equation is a *linear* second-order partial differential equation, whereas the Eikonal equation is a *non-linear* first-order partial differential equation. This distinction gives rise to some interesting properties. First, the potential surface which satisfies the Poisson equation is smoother than that which satisfies the Eikonal equation. The equipotential contour gets smoother as it is closer to the center of the object as opposed to the equidistance contour which is parallel to the boundary [16] (see Figure 11). The potential surface leads to more stable skeletons than those based on the distance transform. Second, in the surface satisfying the Poisson equation, no ridge points are considered separately as in the case with the surface satisfying the Eikonal equation. The two groups are dealt with separately.)
- The gradient of the potential surface, i.e. the electrostatic field, along an equipotential contour reflects the curvature information of the object’s boundary at varying degrees of smoothing. This curvature information is used readily to detect significant convexities and concavities (corners) at different levels of detail and hence, the robustness of the approach in the presence of noise is improved. Field extrema along an equipotential contour correspond to curvature extrema and hence to corners as mentioned in Section III and reported in [1] (see Section III.C). The construction of the potential surface enables the detection of corners at multiple scales [1],[27]. On the contrary, the distance transform does not provide this opportunity, and hence, skeletonization algorithms based on the distance transform must employ a separate technique (e.g. curvature morphology [17]) to detect corners.

VIII. Conclusions and Future Work

In this paper, a novel approach for skeletonization that relies on the EFT has been presented. The background on the EFT that is relevant to the approach has been reviewed. Then, the details of the steps that constitute the proposed skeletonization approach have been presented. The approach has been shown to possess a number of desirable features that can naturally solve many problems that have been encountered with existing skeletonization approaches. First, connectivity and thinness are guaranteed in the proposed approach. Secondly, the EFT approach gracefully captures and unifies notions of corner detection, multiscale, thinning, and skeletonization. Thirdly, the insensitivity of the proposed approach to severe boundary noise has been demonstrated experimentally. Moreover, since the new skeletonization approach is developed based on a well-established theory, the

electrostatic field theory, the performance of the proposed approach under varying conditions can be predicted and justified before experiments are even conducted. Experiments on a synthesized square were performed to illustrate the potential of the proposed approach and its insensitivity to boundary noise. Also the approach was also experimented with a Maple leaf image and results generated by the algorithm are very encouraging.

Our research work using the EFT framework for solving computer vision problems inspires further research using the same approach in addressing other vision problems. Many directions of research based on the EFT can be done. An elegant way to eliminate skeleton branches that pertain to noise can be investigated. Also, a quantitative method by which skeletons generated by the EFT-based skeletonization approach can be evaluated and hence, the refinement of the skeleton can be developed.

The potential distribution in its own constitutes a useful representation of objects at various levels of details similar to the multiscale curvature-based shape representation approach [21], [22]. In the proposed approach, scale is naturally defined by the potential distribution. In fact, the equipotential contours generated from the potential surface can be viewed as fingerprints of the object [25] for robust representation and recognition, the application of which is an interesting research topic.

The problem of skeletonization of objects containing holes are also of major concern and is currently studied by the authors. The definition of the skeleton using the EFT may have to be modified as follows. The skeleton is the union of the zero equipotential (connected) contour(s) (one surrounding each hole) and electrostatic field lines (skeletal branches) originating from significant convexities and concavities along the boundary curve. Finding the zero equipotential contour(s), however, is not an easy task in a digital grid when objects contain narrow regions or *bottle necks* since the space would not be large enough for the potential distribution to fall down to zero because of quantization. A possible solution to this problem is to use the multigrid approach [32] to refine the potential values at the bottle necks and eventually find the zero potential contour(s).

A natural extension to the EFT-based approach is to use it in representing three-dimensional objects because the Poisson equation is general and is not restricted to two dimensions. The potential surface becomes the *potential volume* and the equipotential contours in are replaced by equipotential surfaces. Also, the electrostatic field extrema would correspond to curvature extrema, and hence, three-dimensional edges and three-dimensional corners can be detected using the same methodology described in this paper. Once the potential volume is estimated, the three-dimensional skeleton of a three-dimensional object [9], [23], which has a special importance in biomedical applications, can be extracted .

Another extension to the approach is to extend it to solve the *dynamic scene analysis* problem. In this case, the more general *wave equation* can be used instead of the Poisson equation to model and accommodate for the time variation of the potential distribution.

The most critical step in the proposed approach in terms of the running time performance is the generation of the potential distribution. Non-iterative direct analytical methods for solving the Poisson equation [29] deserve further investigation.

The experience in this work suggests that interesting features exhibited by the electrostatic field-based approach of corner detection and skeletonization promote the investigation of more physics-based models in solving computer vision problems. Finally, it is believed that borrowing simple ideas from other disciplines, such as physics, will certainly benefit research in the computer vision community.

References

- [1] G. H. Abdel-Hamid and Y.-H. Yang, Electrostatic field-based detection of corners of planar curves, in *Proceedings of the 1993 Canadian Conference on Electrical and Computer Engineering*, Vancouver, Canada, Sept. 1993, pp. 767-770.

- [2] C. Arcelli, Pattern thinning by contour tracing, *Comput. Graphics Image Process.*, vol. 17, pp. 130-144, 1981.
- [3] H. Blum, A transformation for extracting new descriptors of shape, in *Models for the Perception of Speech and Visual Form* (W. Wathen-Dunn, ed.), Cambridge MA: MIT Press, 1967.
- [4] J. W. Brandt and V. R. Algazi, Continuous skeleton computation by Voronoi diagram, *CVGIP: Image Understanding*, vol. 55, no. 3, pp. 329-338, 1992.
- [5] G. Chen and Y. -H. Yang, Edge detection by regularized cubic B-spline fitting, Res. Rep. 91-8, University of Saskatchewan, Dept. of Comp. Sc. , Saskatoon, Saskatchewan, Canada, Aug. 1991, to appear in *IEEE Trans. Systems, Man and Cyber.*
- [6] P. E. Danielsson, Euclidean distance mapping, *Comput. Graphics Image Process.*, vol. 14, pp. 227-248, 1980.
- [7] A. R. Dill, M. D. Levine, and P. B. Noble, Multiple resolution skeletons, *IEEE Trans. Patt. Anal. Machine Intell.*, vol. PAMI-9, pp. 495-504, 1987.
- [8] A. J. Baden Fuller, *Engineering Field Theory*, Pergamon Press, Oxford, 1973.
- [9] J. Gauch and S. Pizer, The intensity axis of symmetry and its application to image segmentation, *IEEE Trans. Patt. Anal. Machine Intell.*, vol. PAMI-15, no. 8, pp. 753-770, 1992.
- [10] Z. Guo and R. W. Hall, Fast fully parallel thinning algorithms, *CVGIP: Image Understanding*, vol. 55, no. 3, pp. 317-328, 1992.
- [11] B. K. P. Horn and M. J. Brooks, The variational approach to shape from shading, *Comput. Vision, Graphics, Image Processing*, vol. 33, pp. 174-208, 1986.
- [12] F. Klein and O. Kubler, Euclidean distance transformation and model guided image interpretation, *Patt. Recogn. Lett.*, vol. 3, pp. 19-30, 1987.
- [13] L. Lam and C. Y. Suen, Automatic evaluation of skeleton shapes, in *Proc. 11th Int. Conf. on Pattern Recognition*, The Hague, The Netherlands, 1992, pp. 342-345.
- [14] L. Lam, S.-W. Lee, and C. Y. Suen, Thinning methodologies-a comprehensive survey, *IEEE Trans. Patt. Anal. Machine Intell.*, vol. PAMI-14, no. 9, pp. 869-885, 1992.
- [15] S.-W. Lee, L. Lam, and C. Y. Suen, Performance evaluation of skeletonization algorithms for document image processing, in *Proc. 1st Int. Conf. on Document Analysis and Recognition*, St. Malo, France, Sept. 1991, pp. 260-271.
- [16] F. Leymarie and M. D. Levine, Simulating the grassfire transform using an active contour model, *IEEE Trans. Patt. Anal. Machine Intell.*, vol. PAMI-14, no. 1, pp. 56-75, 1992.
- [17] F. Leymarie, Tracking and describing deformable objects using active contour models, M. Sc. thesis, McGill University, Montreal, Quebec, Canada, 1990.
- [18] M. P. Martinez-Perez, J. Jimenez, and J. L. Navalon, A thinning algorithm based on contours, *Comput. Graphics Image Process.*, vol. 39, pp. 186-201, 1987.
- [19] A. R. Mitchell and D. F. Griffiths, *The Finite Difference Method in Partial Differential Equations*, John Wiley, 1980.
- [20] R. Mittra and S. W. Lee, *Analytical Techniques in The Theory of Guided Waves*, McMillan, New York, pp. 4-11, 1971.

- [21] F. Mokhtarian and A. K. Mackworth, Scale-based description and recognition of planar curves and two-dimensional shapes, *IEEE Trans. Patt. Anal. Machine Intell.*, vol. PAMI-8, no. 1, pp. 34-43, 1986.
- [22] F. Mokhtarian and A. K. Mackworth, A theory of multiscale, curvature-based shape representation for planar curves, *IEEE Trans. Patt. Anal. Machine Intell.*, vol. PAMI-14, no. 8, pp. 789-805, 1992.
- [23] T. Nguyen and J. Sklansky, Reconstructing the 3-D medical axes of coronary arteries in single-view cineangiograms, in *IEEE Trans. Med. Imaging*, vol. 13, no. 1, pp. 61-73, 1994.
- [24] R. Ogniewicz and M. Ilg, Voronoi skeletons: theory and applications, in *Proc. IEEE Conf. on CVPR*, Champaign, Illinois, 1992, pp. 63-69.
- [25] M. A. Piech, Comment on fingerprints of two-dimensional edge models, *Comput. Vision, Graphics and Image Process.*, vol. 42, pp. 381-386, 1988.
- [26] R. Plamondon and C. Y. Suen, On the definition of reference skeletons for comparing thinning algorithms, in *Proc. Vision Interface 1988*, Edmonton, Canada, 1988, pp. 70-75.
- [27] A. Rattarangsi and R. T. Chin, Scale-based detection of corners of planar curves, *IEEE Trans. Patt. Anal. Machine Intell.*, vol. PAMI-14, no. 4, pp. 430-449, 1992.
- [28] B. Shapiro, J. Pisa, and J. Sklansky, Skeleton generation from x, y boundary sequences, *Comput. Graphics Image Process.*, vol. 15, pp. 136-153, 1981.
- [29] T. Simchony, R. Chellappa, and M. Shao, Direct analytical methods for solving Poisson equations in computer vision problems, *IEEE Trans. Patt. Anal. Machine Intell.*, vol. PAMI-12, no. 5, pp. 435-446, 1990.
- [30] R. W. Smith, Computer processing of line images: A survey, *Pattern Recognition*, vol. 20, no. 1, pp. 7-15, 1987.
- [31] I. N. Sneddon, *Elements of Partial Differential Equations*, McGraw-Hill, New York, 1957.
- [32] D. Terzopoulos, Image analysis using multigrid relaxation methods, *IEEE Trans. Patt. Anal. Machine Intell.*, vol. PAMI-8, pp. 129-139, 1986.
- [33] O. E. Vega and Y. -H. Yang, Default shape theory: with application to the computation of the direction of the light source, to appear in *CVGIP: Image Understanding*.

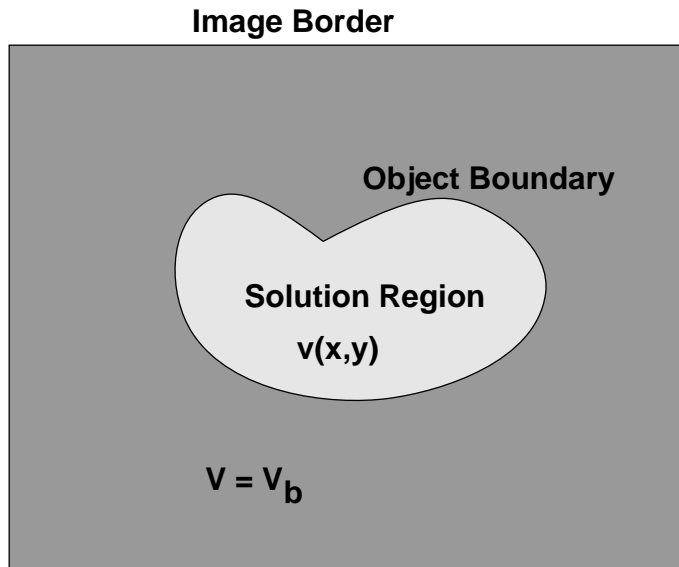


Figure 1: The model of the problem to generate the potential distribution inside the object (the *interior Dirichlet boundary problem*).

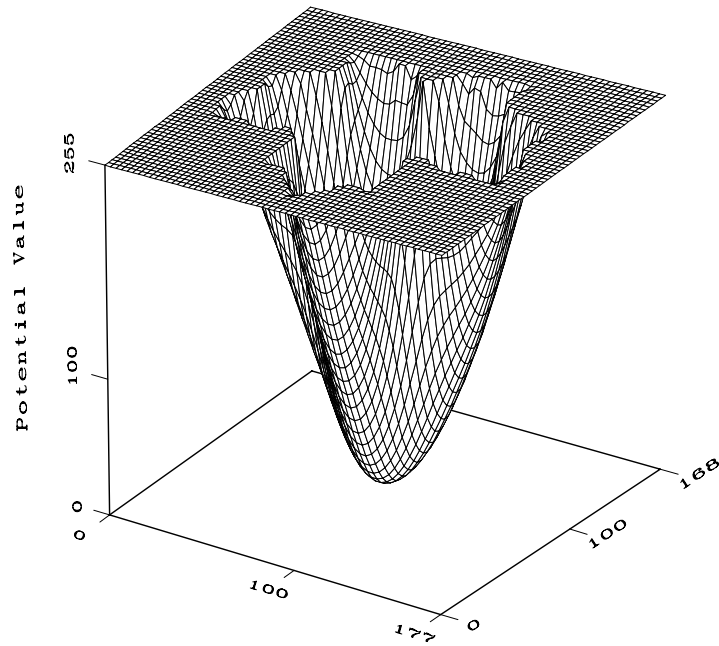
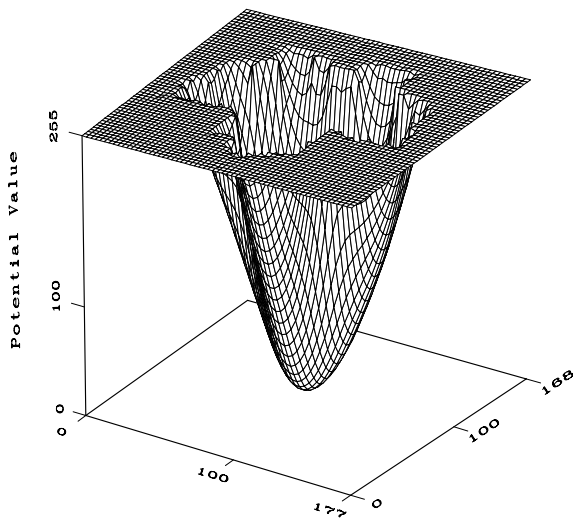
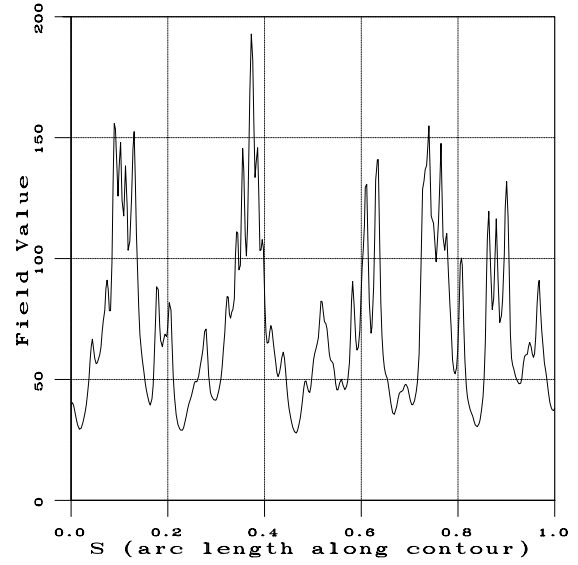


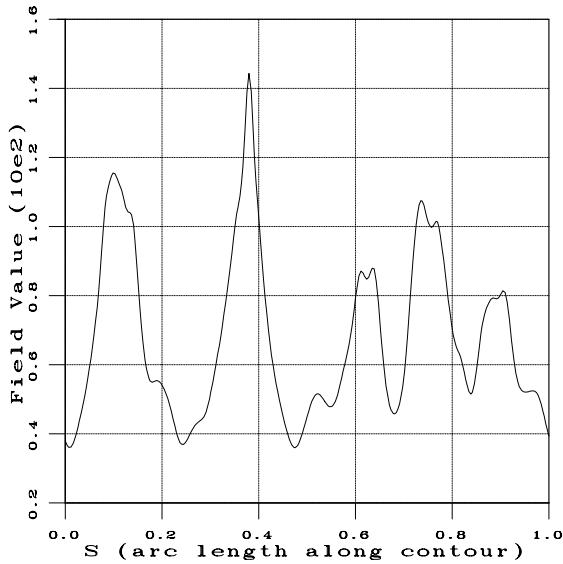
Figure 2: The potential surface generated for the image of a Maple leaf.



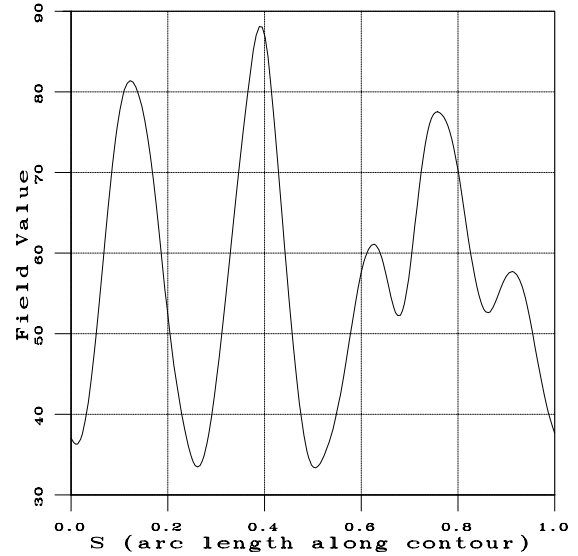
(a)



(b)



(c)



(d)

Figure 3: The smoothing effect on field magnitude at equipotential contours. (a) The potential surface generated for a Maple leaf with boundary corrupted by Gaussian noise of $\sigma = 3$; (b)-(d) Field distribution along equipotential contours of potentials = 230, 180, and 120 respectively. Notice that, the lower the potential, the less the number of field extrema (corresponding to significant convexities and concavities). This illustrates the multiple scale capability of the proposed approach.

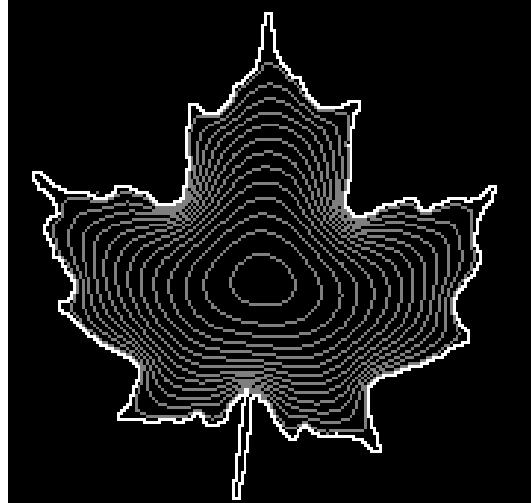


Figure 4: Smoothing effect and multiscale property of equipotential contours. Equipotential contours are constructed for the Maple leaf in Figure 2. The bright contour is the square's boundary. The gray contours are the equipotential contours. The equipotential contours shown are constructed in the potential range 10-250 in steps of 20. When the contour is closer to the center of the object, the contour gets smoother and details tend to disappear.

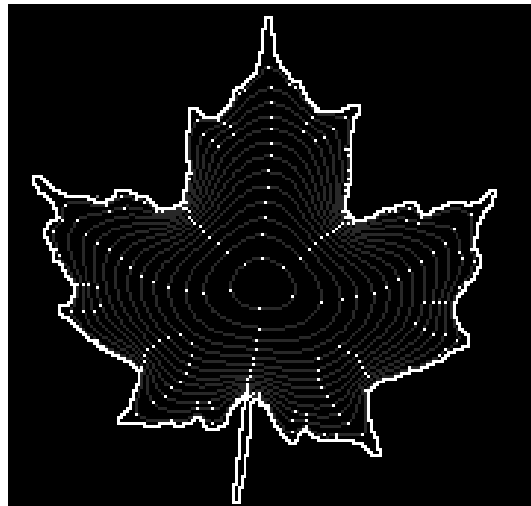


Figure 5: The equipotential contours and their associated corners (bright dots) of the Maple leaf. The contours are constructed for the potential range 10-250 steps of 20. Notice that the number of corners increase with the potential v_{con} .

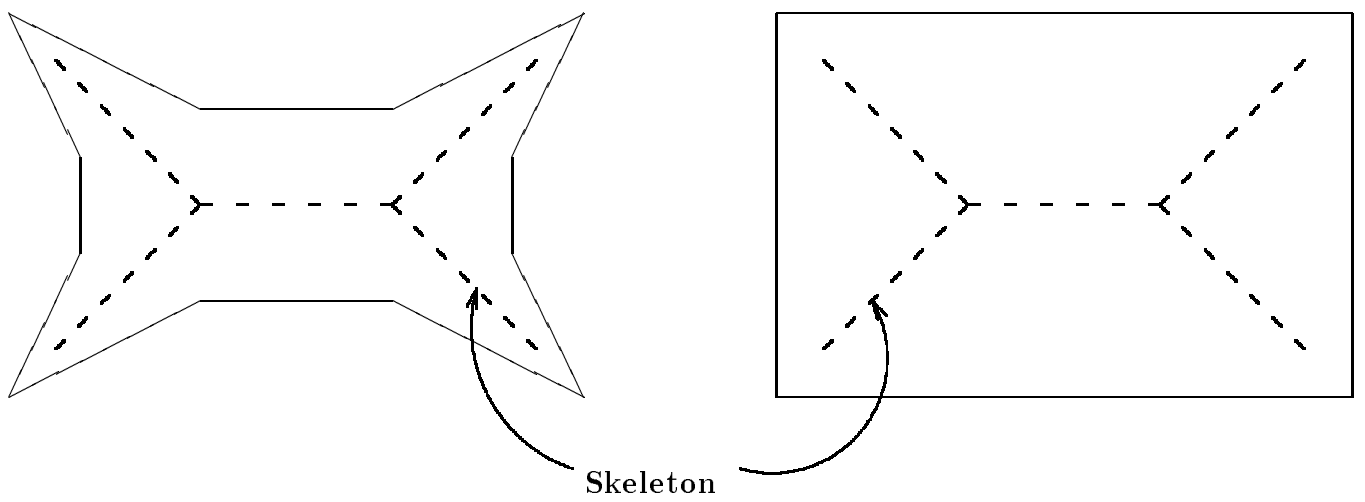


Figure 6: The same skeleton for different shapes. Considering only convexities and disregarding concavities leads to non-unique skeleton representation.

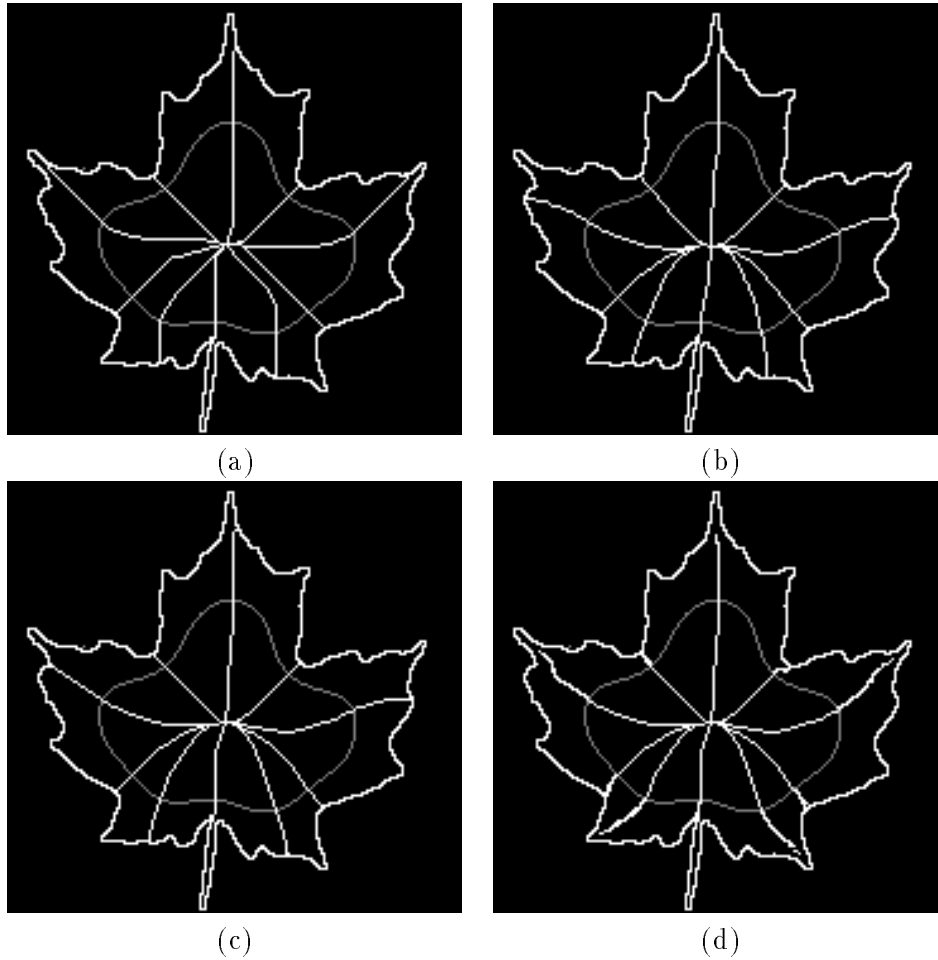


Figure 7: The effect of window size and a refinement of the algorithm in skeleton tracing. produce more accurate field lines. (a) Too small a window (3×3) produces too jaggy skeleton; (b) Too large a window (11×11) leads to inaccurate tracing of field lines; (c) 7×7 window results in a better approximation of field lines; (d) Tracing field extrema along equipotential contours in the outward direction part produces skeletal branches originated from the boundary corners. Three items are shown in the images: (1) the object outline is the exterior contour; (2) the equipotential contour is the interior contour; and (3) the skeleton generated lies inside the object.

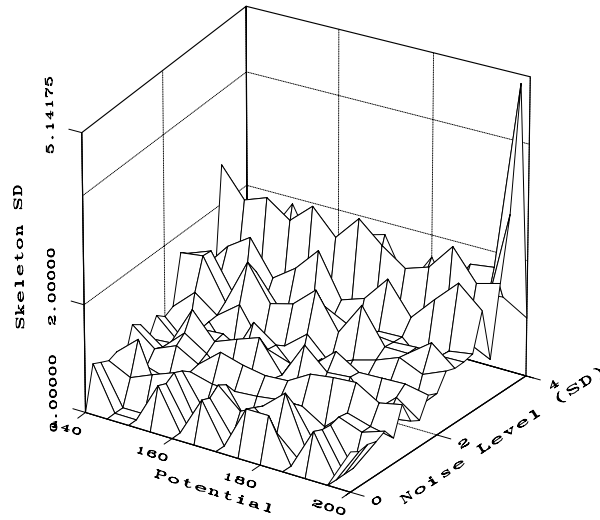


Figure 8: Performance of the proposed skeletonization algorithm with respect to noise. The skeleton SD is used as a figure-of-merit. The experiment is performed on a synthesized square corrupted with a zero-mean Gaussian noise. The performance is measured for a range of starting potentials (140-200) and for a range of boundary noise (0-4). Except for a few erratic points, the skeleton SD is reasonably low.

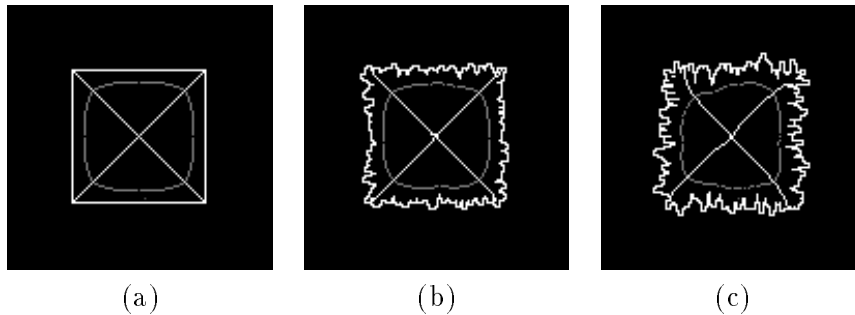


Figure 9: Skeletons generated for a square corrupted with 3 different noise levels 0, 2, and 4. All the three skeletons are started at the equipotential contour of 170. The difference between the ideal (noise-free) skeleton and the generated skeletons is very small.

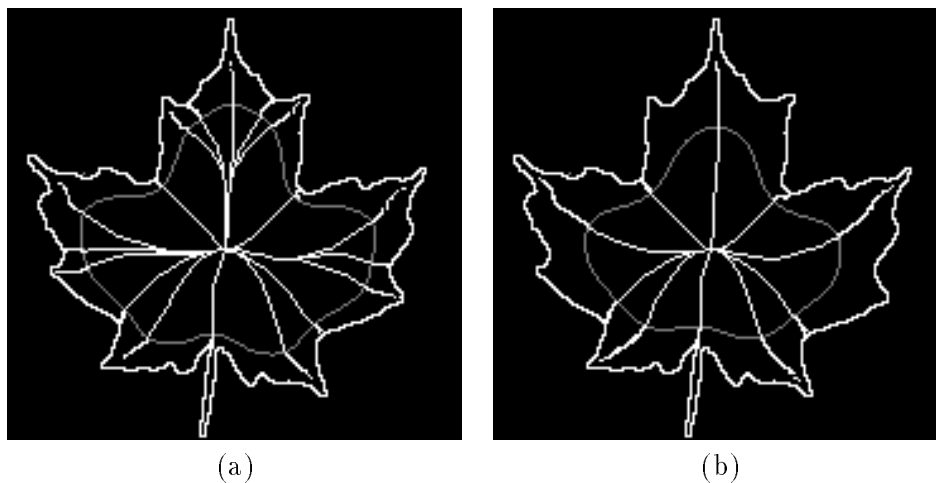
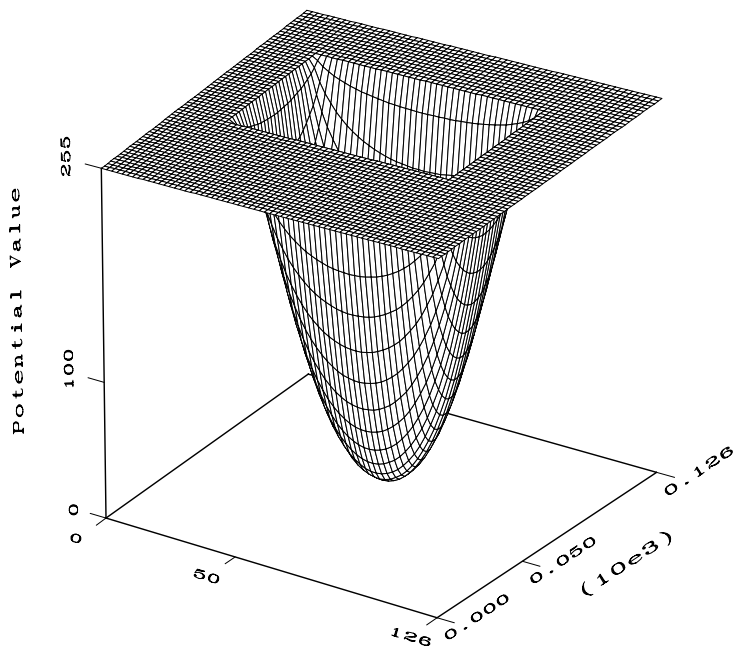
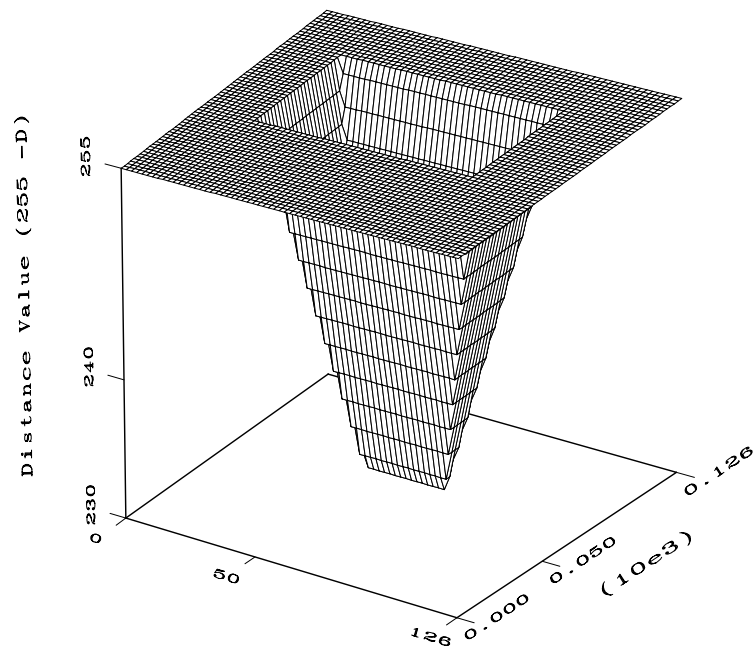


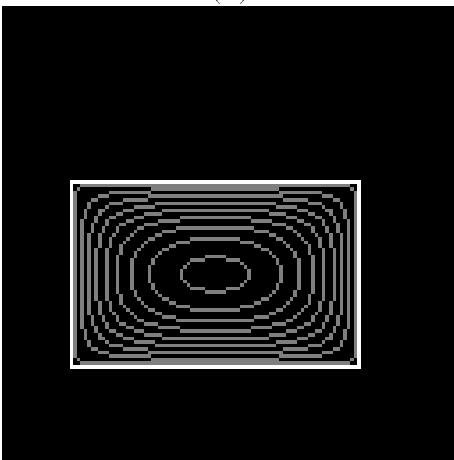
Figure 10: The multiscale capability of the proposed approach. Figure illustrates skeletons generated for a Maple leaf at two different starting equipotentials. (a) 190; (b) 150. The skeleton in (a) has more branches than that of (b). The skeleton in (a) has 18 branches, whereas that in (b) only has 10 branches. The skeleton in (a) represents the leaf at a fine detail, while that in (b) represents the leaf at a coarse detail.



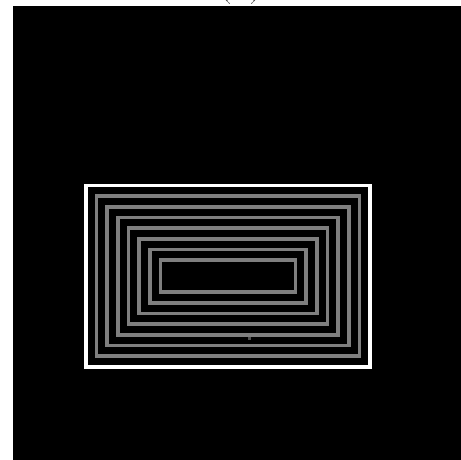
(a)



(b)



(c)



(d)

Figure 11: Comparison between the potential distribution (Poisson's equation) and the distance transform (the Eikonal equation). (a) The potential distribution $v(x, y)$ for a rectangle; (b) The distance transform $D(x, y)$ for the same object; (c) Equipotential contours of the rectangle constructed at the potential range (10-250 in steps of 30 potential unit); (d) Equidistance contours constructed at the distance range 252-232 in steps of 3 pixels. Comparing (a) & (b), it is evident that the potential distribution is much smoother than the distance transform. Moreover, comparing (c) & (d) the equipotential contours represent the object at different levels of details which gives rise to the multiscale property of the proposed skeletonization approach.